Electronic Supplementary Information

Performance and Limits of 2.0 eV Bandgap $CuInGaS_2$ Solar Absorber Integrated with CdS Buffer on $F:SnO_2$ Substrate for Multijunction Photovoltaic and Photoelectrochemical Water Splitting Devices

Nicolas Gaillard,[1,] Wilman Septina, [1] Joel Varley,[2] Tadashi Ogitsu,[2] Kenta K. Ohtaki,[3] Hope A. Ishii,[3] John P. Bradley,[3] Christopher Muzzillo,[4] Kai Zhu,[4] Finn Babbe[5] and Jason Cooper. [5]*

[1] Hawaii Natural Energy Institute, University of Hawaii, Honolulu, Hawaii 96822, USA

[2] Lawrence Livermore National Laboratory, Livermore, California 94550, USA

[3] Hawaii Institute of Geophysics & Planetology, University of Hawaii, Honolulu, Hawaii 96822, USA

[4] National Renewable Energy Laboratory, Golden, Colorado 80401, USA

[5] Chemical Sciences Division, Lawrence Berkeley National Laboratory, Berkeley, CA 94720, USA

* Corresponding author: ngaillar@hawaii.edu

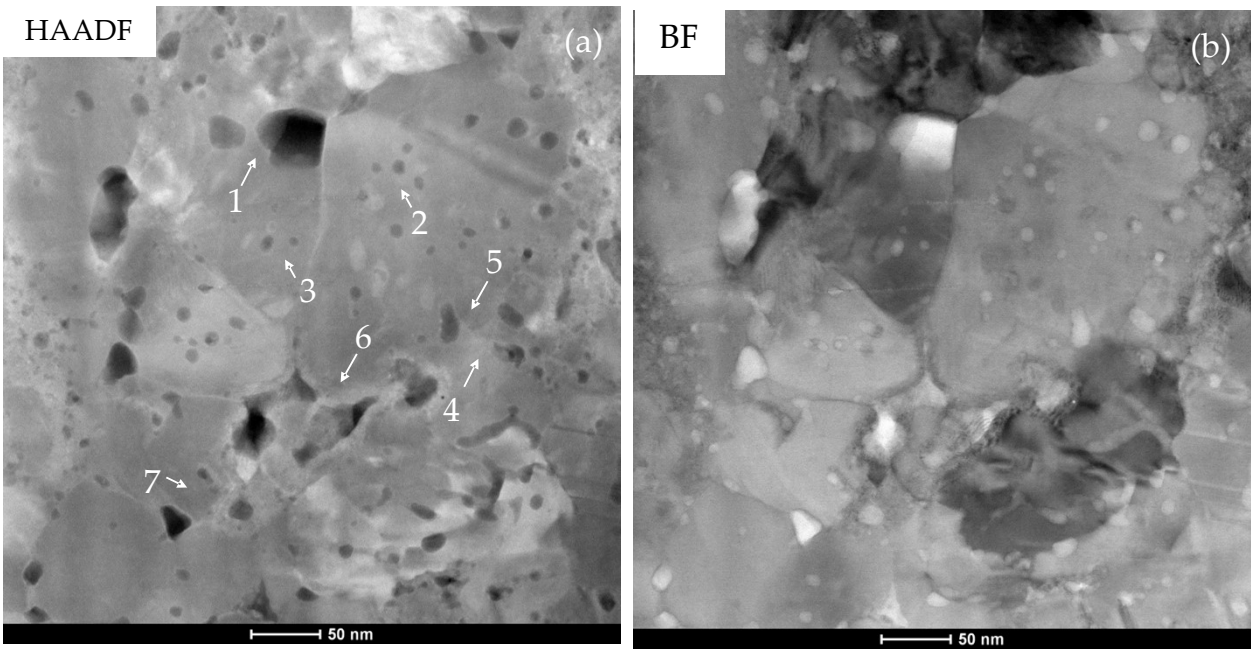

Figure S1. (a) Dark field and (b) corresponding bright field TEM micrographs of the bulk of a CIGS solar cell.

Table S1. Elemental composition measured by TEM/EDX point analysis in Figure S1.

Atomic %	Spot #1	Spot #2	Spot #3	Spot #4	Spot #5	Spot #6	Spot #7	Average
O(K) (%)	31.22	42.13	38.96	33.15	36.81	40.79	34.93	36.9
S(K) (%)	32.62	27.45	28.35	29.65	29.64	28.42	31.26	29.6
Cu(K) (%)	17.02	12.82	13.63	15.84	14.86	12.61	15.09	14.6
Ga(K) (%)	13.03	11.19	12.24	12.4	12	12.08	12.34	12.2
Se(K) (%)	1.55	2.04	2.06	1.53	1.48	1.94	1.48	1.7
Cd(K) (%)	0.27	0.59	0.55	0.6	0.68	0.58	0.63	0.6
In(K) (%)	4.26	3.75	4.17	6.79	4.5	3.56	4.23	4.5
CGI	**0.98**	**0.86**	**0.83**	**0.83**	**0.90**	**0.81**	**0.91**	**0.87**
GGI	**0.75**	**0.75**	**0.75**	**0.65**	**0.73**	**0.77**	**0.74**	**0.73**
SSSe	**0.95**	**0.93**	**0.93**	**0.95**	**0.95**	**0.94**	**0.95**	**0.94**

Room temperature PL data and calibration process:

Photoluminescence spectra were collected at room under various excitation densities using a 405 nm CW laser. An exemplary spectrum is depicted in Figure S6(a) showing a broad asymmetric peak centered around 1.4 eV likely corresponding to a defect-band transition. To determine the external radiative efficiency a reference sample (perylene in ethanol) with a known ERE close to 100 % is used. From the ratio of the excitation density used ($^{EX_{CIGs}}$ and $^{EX_{PL}}$) and the ratio of the integrated PL intensity ($^{Ex_{CIGS}}$, $^{Ex_{PL}}$) as well as the absorptivity of the reference at 405 nm, the ERE of the CIGS can be calculated, giving a value around 0.00012 %.

$$ERE_{CIGS} = \frac{Ex_{CIGS}}{Ex_{Ref}} * \frac{PL_{CIGS}}{PL_{ref}} * abs * ERE_{Ref}$$

This ERE corresponds to a $qFLs_{loss}$ of 0.34 eV [$qFLs_{loss}$ = kT/q * ln(ERE)]. Using the maximal achievable $V_{OC,SQ}$ (1.672 eV) for an Eg of 1.98 eV the qFLs can be determined to be 1.332 eV (high excitation). In the next step the area of the laser spot and total laser power is measured to determine the photon flux density at the sample spot. From this the equivalent number of suns is determined to be ~95 suns by dividing the incoming photon flux by the photon flux absorbed under AM1.5 illumination by an 2 eV bandgap assuming unity absorption above Eg. The qFLs increases with excitation density dependent on the diode factor (as the Voc also does). To extract the optical diode factor, PL is measured over two orders of magnitude and the integrated PL fitted linearly in a log-log plot as shown inf Figure S6(b). The slope gives the optical diode factor of 1.38. In a last step the qFLs value at 95 suns is scaled down by 162 meV corresponding to 1.38*kT/q*ln(95), giving the final qFLs value at 1 sun of (1.17 ± 0.05) eV.

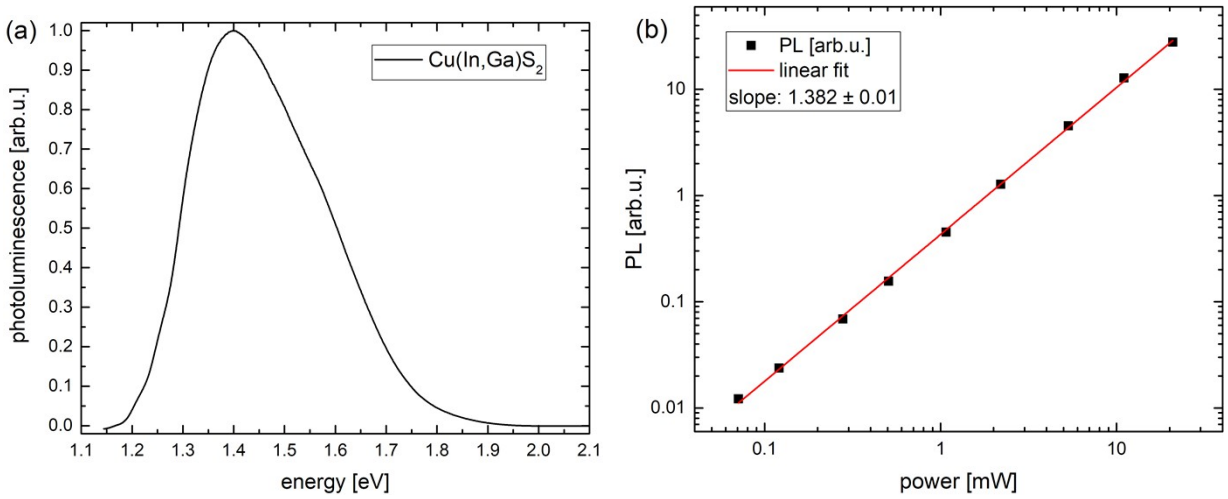

Figure S2: (a) Photoluminescence spectrum of a Cu(In,Ga)S2 absorber layer measured at room temperature with 405 nm excitation. (b) Log-log plot of the integrated PL intensity measured over 2.5 decades of excitation. The slope of the linear fit gives the optical diode factor.

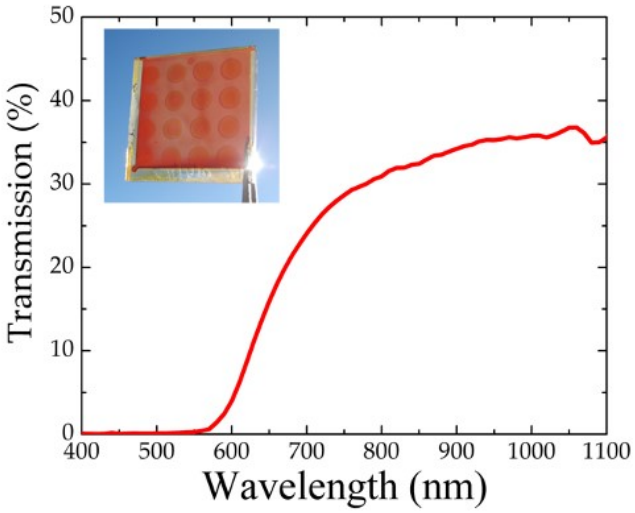

Figure S3. Optical transmission of a fully integrated 2.0 eV CIGS solar cell. (Insert) Optical image of the 1"×1" FTO substrate with nine functional 0.12 cm^2 CIGS solar cells, as defined by ITO pads sputtered through a shadow mask. Cells from the bottom row and left column were shunted due to direct contact of the ITO pads edge with the FTO substrate.

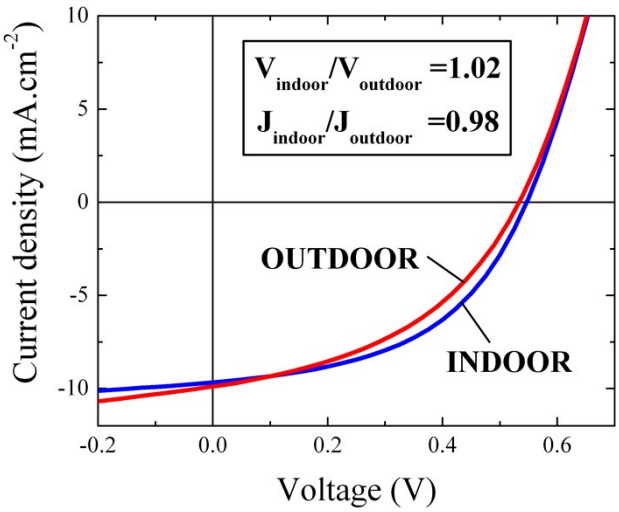

Figure S4. Current vs. voltage characteristics of a representative 2.0 eV CIGS solar cell (PCE = 2.4%) integrated on FTO and measured under simulated ("indoor") and outdoor $AM1.5_G$ illumination. For indoor testing, the J-V characteristic was measured with illumination produced by a 1000W Xe-arc bulb tuned such that its irradiance corresponds to that of $AM1.5_G$ within the absorption range of a 2.0 eV material (375 W/m^2). For outdoor testing, the J-V characteristic was measured when an NREL-calibrated silicon photodiode produced its $AM1.5_G$-calibrated short-circuit current.

Table S2. Temperature-dependence of 1.2eV CIGSe/Mo solar cell electrical properties

T (K)	J_{SC} (mA/cm^2)	V_{OC} (mV)	FF (%)	PCE (%)	R_S ($\Omega.cm^2$)	R_{SH} ($\Omega.cm^2$)	$J_{0,dark}$ (mA/cm^2)	A_{dark}
300	32.9	674	67	14.8	1.79	1020	5.4E-07	1.5
250	33.3	773	69	17.8	1.86	971	2.3E-09	1.6
200	33.2	855	71	20.1	1.81	947	3.8E-09	1.9
150	32.9	931	69	21.1	1.94	842	6.7E-12	2.1

Table S3. Temperature-dependence of 2.0eV CIGS/FTO solar cell electrical properties

T (K)	J_{SC} (mA/cm^2)	V_{OC} (mV)	FF (%)	PCE (%)	R_S ($\Omega.cm^2$)	R_{SH} ($\Omega.cm^2$)	$J_{0,dark}$ (mA/cm^2)	A_{dark}
300	9.37	495	38	1.78	10.57	202	2.0E-03	2.3
250	9.10	595	38	2.03	10.76	249	7.6E-04	2.9
200	7.52	640	35	1.69	19.43	224	1.7E-05	2.5
150	4.49	602	33	0.89	41.43	230	9.1E-07	2.4

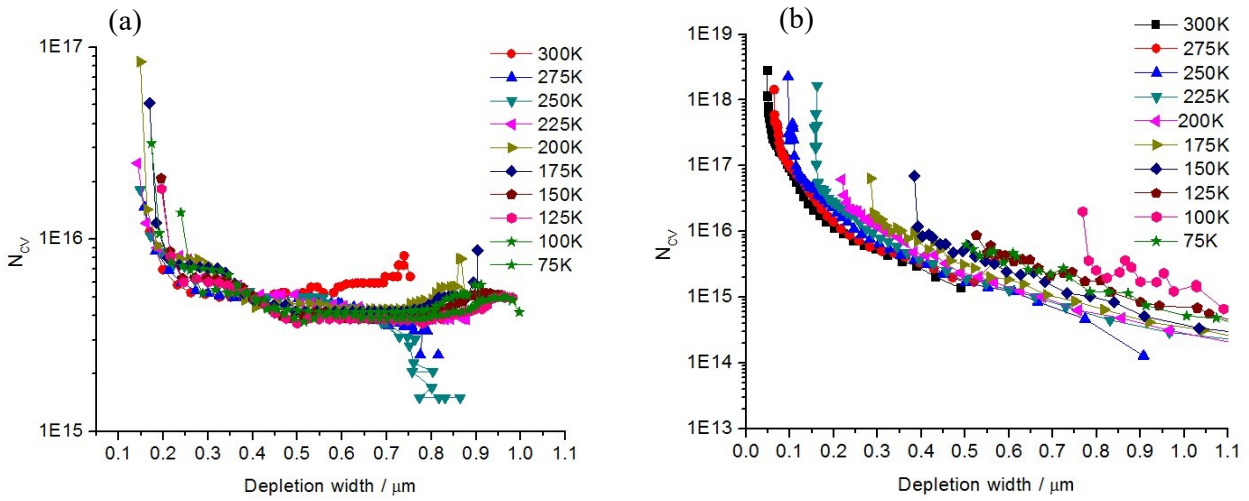

Figure S5. Comparison of the depth profiles of apparent doping density deduced from C-V measurements of (a) 1.13 eV CIGSe and (b) 2.0 eV CIGS solar cells.

Table S4. Apparent doping density (N_{CV}) and depletion width calculated at 0V from the C-V measurements presented in Figure 8.

	1.13 eV $CuInGaSe_2$		2.0 eV $CuInGaS_2$	
T	x at 0V (μm)	Ncv at 0V	x at 0V (μm)	Ncv at 0V
300	0.39	5.19E+15	0.06	3.67E+17
275	0.4	4.95E+15	0.08	2.23E+17
250	0.39	5.34E+15	0.11	1.40E+17
225	0.39	5.16E+15	0.16	1.05E+17
200	0.4	4.43E+15	0.22	6.20E+16
175	0.44	4.57E+15	0.29	1.92E+16
150	0.51	3.99E+15	0.39	1.19E+16
125	0.58	4.01E+15	0.55	4.72E+15
100	0.52	3.87E+15	0.78	3.61E+15
75	0.45	4.32E+15	-	-

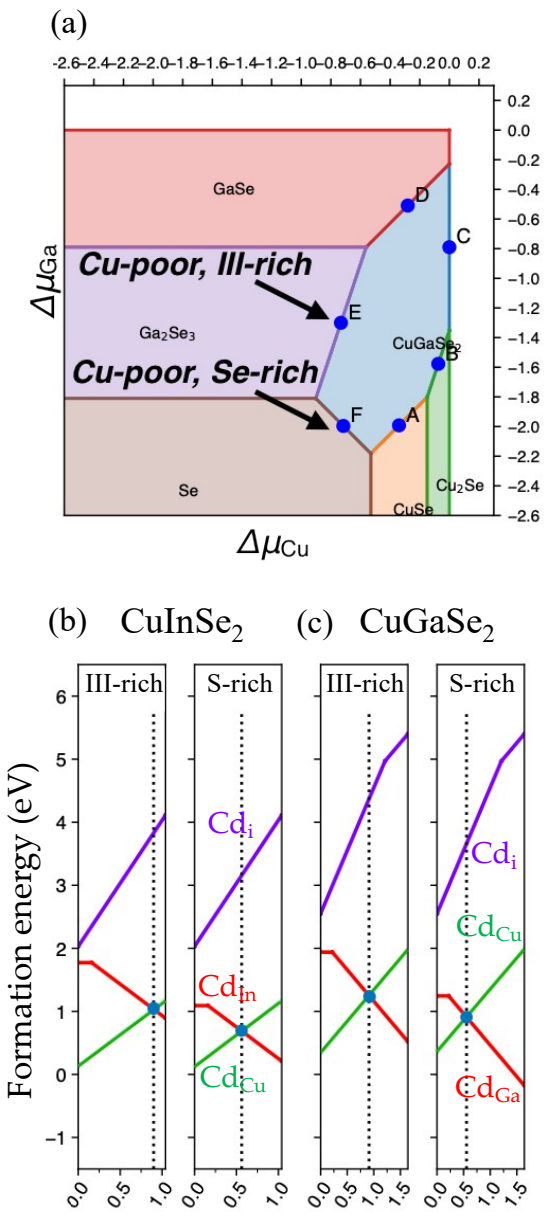

Figure S6. (a) Representative chalcopyrite phase diagram for $CuGaSe_2$, shown as a function of the Ga and Cu chemical potentials (μ). The calculated formation energies of dilute Cd impurities are included for $CuInSe_2$ (b) and $CuGaSe_2$ (c), shown for conditions representing the regimes of Cu-poor and III-rich/Se-poor and Se-rich/III-poor limits, as highlighted in (a). The Fermi level that would result from self-compensation from Cd incorporation is included as the dashed lines in (b) and (c). In contrast the sulfides, these Fermi level values are nearly identical for $CuInSe_2$ and $CuGaSe_2$, indicating little sensitivity to the Cd-related Fermi-level pinning values to the GGI in CIGSe alloys.

Table S5. Summary of formation enthalpies (eV/formula unit) for phases considered in the construction of the calculated phase diagrams in the main text. Chemical potentials (μ_i) of the parent compounds (elemental Cu, Ga, In, Se, S and Cd) were defined relative to the energy per atom in their bulk elemental phases.[1,2]

Alloy	Formation enthalpy (eV/ formula unit)	Alloy	Formation enthalpy (eV/ formula unit)	Alloy	Formation enthalpy (eV/ formula unit)
CuInS2	-2.541	CuInSe2	-2.483	CuIn3Se5	-5.302
CuGaS2	-3.028	CuGaSe2	-2.712	CuIn3S5	-5.526
CuIn5S8	-9.234	CuIn5Se8	-8.836	CuGa3Se5	-6.019
CuGa5S8	-11.073	CuGa5Se8	-9.833	CuGa3S5	-6.884
CuSe	-0.53	Cu2Se	-0.68	Cu3Se2	-1.12
CuS2	-0.152	CuS	-0.535	Cu2S	-0.994
In2S3	-3.3	In2Se3	-3.25		
Ga2S3	-3.952	Ga2Se3	-3.62		
InS	-1.189	InSe	-1.28		
GaS	-1.526	GaSe	-1.47		

References

[1] Pohl, J. & Albe, K. Intrinsic point defects in CuInSe2 and CuGaSe2 as seen via screened-exchange hybrid density functional theory. Phys Rev B 87, 245203 (2013).

[2] Jain, A., Ong, S. P., Hautier, G., Chen, W., Richards, W. D., Dacek, S., Cholia, S., Gunter, D., Skinner, D., Ceder, G. & Persson, K. A. Commentary: The Materials Project: A materials genome approach to accelerating materials innovation. Apl Mater 1, 011002 (2013).